OPEN ACCESS

University of BRISTOL

Pereira, G. C., Pereira, S. P., Pereira, F. B., Lourenço, N., Lumini, J. A., Pereira, C. V., Bjork, J. A., Magalhães, J., Ascensão, A., Wieckowski, M. R., Moreno, A. J., Wallace, K. B., & Oliveira, P. J. (2019). Early Cardiac Mitochondrial Molecular and Functional Responses to Acute Anthracycline Treatment in Wistar Rats. *Toxicological Sciences*, *169*(1), 137-150. https://doi.org/10.1093/toxsci/kfz026

Peer reviewed version

Link to published version (if available):
10.1093/toxsci/kfz026

Link to publication record in Explore Bristol Research
PDF-document

This is the author accepted manuscript (AAM). The final published version (version of record) is available online via University of Oxford Press at https://academic.oup.com/toxsci/article/169/1/137/5304396. Please refer to any applicable terms of use of the publisher.

University of Bristol - Explore Bristol Research
General rights

This document is made available in accordance with publisher policies. Please cite only the published version using the reference above. Full terms of use are available:
http://www.bristol.ac.uk/red/research-policy/pure/user-guides/ebr-terms/

Early Cardiac Mitochondrial Molecular and Functional Responses to Acute Anthracycline Treatment in Wistar Rats

Gonçalo C. Pereira[1,a,#], Susana P. Pereira[1,b], Francisco B. Pereira[2,3], Nuno Lourenço[2], José A. Lumini[4,5,6], Claudia V. Pereira[1,c], James A. Bjork[7], José Magalhães[4], António Ascensão[4], Mariusz R. Wieckowski[8], António J. Moreno[1,9], Kendall B. Wallace[7] and Paulo J. Oliveira[1].

1. CNC - Center for Neuroscience and Cell Biology, University of Coimbra, UC-Biotech, Biocant Park, Cantanhede, Portugal
2. Centre for Informatics and Systems, University of Coimbra, Polo II, Pinhal de Marrocos, Coimbra, Portugal
3. Coimbra Polytechnic - ISEC, Coimbra, Portugal
4. Research Centre in Physical Activity, Health and Leisure, Faculty of Sport Sciences, University of Porto, Porto, Portugal
5. Faculty of Health Sciences, University of Fernando Pessoa, Porto, Portugal.
6. LABIOMEP - Porto Biomechanics Laboratory, Porto University, Porto, Portugal
7. Department of Biomedical Sciences, University of Minnesota Medical School, Duluth, Minnesota, USA
8. Nencki Institute of Experimental Biology, Warsaw, Poland
9. Department of Life Sciences, University of Coimbra, Coimbra, Portugal

Current addresses:
a – School of Biochemistry, University Walk, University of Bristol, Bristol, UK
b – Research Centre in Physical Activity Health and Leisure (CIAFEL), Faculty of Sports, University of Porto, Porto, Portugal
c - University of Miami Miller School of Medicine, Neurological Research Building, Miami, FL, USA

Corresponding author:

Gonçalo Pereira, PhD
Current Address: School of Biochemistry, University Walk, University of Bristol, Bristol BS8 1TD
g.pereira@bristol.ac.uk

ORCID:
Gonçalo C. Pereira (0000-0001-9638-0615), Susana P. Pereira (0000-0002-1168-244) Francisco B. Pereira (0000-0002-1937-6548), Nuno Lourenço (0000-0002-2154-0642), José A. Lumini (0000-0003-1565-7075), Claudia V. Pereira (0000-0001-5666-5720.), James A. Bjork (n.a.), José Magalhães (0000-0003-4808-8374), António Ascensão (0000-0001-5269-0857), Mariusz R. Wieckowski (0000-0003-0789-4521), António J. Moreno (0000-0003-3575-7604), Kendall B. Wallace (n.a.) and Paulo J. Oliveira (0000-0002-5201-9948).

Keywords: doxorubicin; animal study; cardiotoxicity; mitochondrial permeability transition; principal component analysis; feature correlation analysis

Abbreviations List: ADP – adenosine diphosphate; CsA – cyclosporin A; DOX – doxorubicin; EGTA – ethylene glycol tetraacetic acid; mPTP - mitochondrial permeability transition pore; OXPHOS – oxidative phosphorylation; ROS – reactive oxygen species.

ABSTRACT

Doxorubicin (DOX) is an anticancer drug widely used to treat human and non-human tumors but the late and persistent cardio-toxicity reduces the therapeutic utility of the drug. The full mechanism(s) of DOX-induced acute, sub-chronic and delayed toxicity, which has a preponderant mitochondrial component, remains unclear; therefore, it is clinically relevant to identify early markers to identify patients who are predisposed to DOX-related cardiovascular toxicity.

To address this, Wistar rats (16 weeks old) were treated with a single DOX dose (20 mg/Kg, i.p.); then, mRNA, protein levels and functional analysis of mitochondrial end-points were assessed 24 h later in the heart, liver and kidney. Using an exploratory data analysis, we observed cardiac-specific alterations after DOX treatment for mitochondrial Complexes III, IV, and preferentially for Complex I. Conversely, the same analysis revealed Complex II alterations are associated with DOX response in the liver and kidney. Interestingly, H_2O_2 production by the mitochondrial respiratory chain as well as loss of calcium-loading capacity, markers of sub-chronic toxicity, were not reliable indicators of acute DOX cardiotoxicity in this animal model.

By using sequential Principal Component Analysis and Feature Correlation Analysis, we demonstrated for the first time alterations in sets of transcripts and proteins, but not functional measurements, that might serve as potential early acute markers of cardiac-specific mitochondrial toxicity, contributing to explain the trajectory of DOX cardiac toxicity and to develop novel interventions to minimize DOX cardiac liabilities.

INTRODUCTION

Doxorubicin (DOX) is an anthracycline antibiotic that is widely used as a chemotherapeutic agent to treat multiple types of cancers (Simunek *et al.*, 2009; Sterba *et al.*, 2013); however, its therapeutic utility is limited due to the development of a cumulative and dose-dependent cardiotoxicity (Wallace, 2007). Congestive heart failure after DOX treatment is a pressing concern. The mortality observed after a chronic treatment can be as high as 50% (Chatterjee *et al.*, 2010), increasing significantly for cumulative doses higher than 500 mg/m^2 as reported by Singal *et al.* (1998). This life-time cumulative dose is equivalent to 13.5 mg/Kg_{humans} or 83.8 mg/Kg_{rats}, using reference values and calculations suggested by Nair *et al.* (2016). The etiology of DOX-induced cardiotoxicity is commonly ascribed to a redox-cycling of the drug on Complex I of the mitochondrial respiratory chain (Davies *et al.*, 1986). Reactive oxygen species (ROS) generated during this process are believed to be responsible for the toxic effects on cardiac mitochondria, resulting in impaired oxidative phosphorylation (Santos *et al.*, 2002), loss of mitochondrial calcium homeostasis (Zhou *et al.*, 2001a) and increased apoptotic signaling (Childs *et al.*, 2002). DOX cardiotoxicity can present distinct phenotypes depending on the time elapsed since the initial treatment. Among the wide range of treatment protocols used in different laboratories (Ascensao *et al.*, 2012; Hayward *et al.*, 2007; Solem *et al.*, 1996; Zhou *et al.*, 2001c) we have previously demonstrated that treating Wistar rats with DOX resulted in toxicity only in the cardiac tissue and more easily detected in a sub-chronic treatment protocol (Pereira *et al.*, 2012).

A distinguishing feature is the fact that DOX toxicity presents a delayed component, manifesting itself years or even decades after treatment (Steinherz *et al.*, 1991). Despite the abundant research in the last decades, the mechanism(s) underlying delayed DOX cardiac toxicity evolution are still far from being understood. Regardless the mechanism(s), it is clinically relevant to identify early signs of specific metabolic or transcriptional alterations observed after acute DOX treatment that may be considered early stress response(s). For this objective, we measured three distinct sets of data on cardiac, renal, and hepatic tissue in a rat model subjected to an acute DOX treatment (Ascensao, et al., 2012; Pereira, et al., 2012):

(i) mRNA and protein levels of subunits of the mitochondrial respiratory complexes (I-IV), ATP synthase, and other relevant mitochondrial components (Cyt c, ANT, VDAC), and applied a suite of exploratory data analysis tools in clusters of transcripts related to the same complex. From this use we seek to obtain

92 evidence of DOX-induced acute alterations that are present even in the absence of significant differences
93 in the overall respiration flux (Pereira *et al.*, 2016).
94 (ii) hydrogen peroxide (H_2O_2) production by the mitochondrial respiratory chain.
95 (iii) the sensitivity to the mitochondrial permeability transition (mPTP) as a surrogate of DOX response.
96 Since the latter markers have both been detected in sub-chronic DOX toxicity animal models (Cappetta *et al.*,
97 2017; Zhou, et al., 2001c), our objective was to measure similar alterations in the acute model, with the
98 novelty of performing experiments with both Complex I and II substrates.
99 We used in this study a Wistar rat-based animal model and the acute treatment protocol previously described
100 (Pereira, et al., 2012). A single dose of 20 mg/Kg DOX caused an increase in circulating troponin I and a ~
101 7.6 % decrease in cardiac mass with no visible alterations on the mitochondrial functional parameters
102 evaluated. However, if a similar dosage was spanned over the period of 7 weeks (sub-chronic model), a clear
103 mitochondrial impairment was observed (Pereira, et al., 2012; Zhou, et al., 2001a; Zhou *et al.*, 2001b; Zhou,
104 et al., 2001c), suggesting that DOX acute effects may progress into mitochondrial bioenergetic dysfunction.
105 Moreover, it also suggests that the acute DOX toxicity model may be used to assess mitochondrial alterations
106 that precede functional changes. Therefore, we included mitochondrial molecular parameters in the present
107 study and anticipated that our novel approach will allow the assessment of early markers of acute DOX
108 cardiotoxicity, facilitating the development of biomarkers to be used in the clinic for timely identification of
109 patients with higher susceptibility to latent DOX toxicity and for the development of interventions aimed at
110 decreasing DOX off-target cardiac toxicity.
111

RESULTS

Exploratory Data Analysis

In the present research, we applied Principal Component Analysis (PCA) and Feature Correlation Analysis (FCA) to discover correlations and clustering patterns that help to identify relevant mitochondrial markers for the early detection of acute DOX toxicity. The small number of available samples prevents a complete and robust statistical analysis of the results. However, PCA provides initial insight regarding the separation of the treatment groups (Saline vs. DOX) allowing the discovery of important relevant trends. The twelve panels from Figure 1 illustrate the separation between Saline and DOX samples, for each of the 4 mitochondrial respiratory complexes in heart, kidney and liver tissues, respectively. To allow an informative 2D visualization we considered just the two principal components (explaining > 70% of the variance) and projected the original data in the lower dimensional space.

Considering the cardiac tissue (Fig. 1a), the four panels representing each of the respiratory complexes tend to exhibit a clear separation between areas comprising samples from saline (blue area) and DOX-treated rats (red area). The separation is clearly visible for Complex I while some minor perturbations are observed in Complexes II, III, and IV. These minor differences correspond to specific regions where the separation is not evident, suggesting that it might be difficult for a computational analysis to accurately classify examples in these locations. Class separation between treatment groups for some respiratory complexes is also less evident when analyzing the remaining tissues in the study. For example, when analyzing the renal tissue (Fig. 1b) a visible class separation in Complexes II and III was observed, but the other complexes displayed several mixed sub-areas that might compromise the correct identification of the samples. Similarly, Complex II in the hepatic tissue (Fig. 1c) tends to generate a clear boundary between the two treatment groups, while the other complexes reveal several density sub-areas.

Overall, PCA analysis of mRNA transcripts identified Complex I as preferable target for DOX acute toxicity in the heart while Complex II preferentially relates to DOX effects in the liver and kidney. Complexes III and IV are not robust markers to differentiate DOX toxicity in the analyzed tissues of this study.

Next, we complemented the PCA with individual FCA, to estimate the dependence that may exist between every pair of features. Our analysis considered all pairwise feature correlations and aimed to identify variables

exhibiting high sensitivity to DOX. Figure 2a-c show the global trend in the correlation changes resulting from DOX administration for features describing mRNA and protein levels in the heart, kidney and liver tissues, respectively.

Observationally, there are some noticeable differences in the global patterns shown in Fig.2. In regard to liver (Fig. 2c), DOX administration tends to have a minor impact in the correlation strength change (high number of blank cells). Nonetheless, there is a high and consistent change involving the expression of subunit NDUFB8 in the liver. Conversely, Figures 2a and 2b, representing heart and kidney, respectively, exhibit a considerable number of filled cells identifying pairs with sizable correlation changes. The correlation change of NDUFB8 that was signaled in the liver is also present in these tissues, although to a lesser extent.

Regarding features from Complex I, some additional correlation changes are observed, namely *ND1* and *ND2* mRNA in the kidney and *ND6* and *NDUFS4* mRNA in the heart.

In respect to Complex II, no noticeable changes in correlation were observed, regardless of the tissue in study.

In Complex III related features, DOX treatment showed a stronger effect on the correlation change of CytB mRNA and UQCRFS1 protein levels in kidney. Finally, a few correlation changes regarding Complex IV features were also observed in heart and kidney, but not as obvious as reported above (Fig. S1).

Overall, the FCA analysis suggests that the impact of the DOX treatment is easier to perceive if considering samples from heart and kidney when compared to liver, in agreement with findings obtained from PCA.

Mitochondrial hydrogen peroxide production

DOX-induced oxidative stress is considered a hallmark of its toxicity (Pereira, et al., 2012). In the present work, we investigate the contribution of different sites of the mitochondrial respiratory chain to the overall oxidative response by DOX. In respect to Complex I-sustained respiration, H_2O_2 production was similar to control values in heart and kidney mitochondria regardless of the energization conditions tested (Fig. 3a, c). However, in liver mitochondria, H_2O_2 production in the presence of rotenone was higher in mitochondria from DOX-treated animals (11 ± 3%) even though no statistical differences were observed in the presence of antimycin A alone (18 ± 10%) or with antimycin A plus rotenone (1 ± 2%).

When mitochondria were energized with Complex II-linked substrates, heart mitochondria from DOX-treated animals showed increased production of H_2O_2 in the presence of substrate alone, yet it was not statistically

168 significant (164 ± 72%, p = 0.06; Fig. 3a). Interestingly, this alteration was only observed in the absence of
169 respiratory chain inhibitors as other conditions were similar to controls, reflecting ROS production through
170 reverse electron transfer.
171 In regard to liver and kidney, mitochondria from DOX-treated animals energized with Complex II-linked
172 substrates presented similar levels of H_2O_2 production under all tested conditions (Fig. 3b, c).
173 Overall, liver mitochondria from DOX-treated animals appear to generate more H_2O_2 compared to heart or
174 kidney mitochondria but only when the respiratory chain is challenged by oxidative phosphorylation
175 (OXPHOS) inhibitors, suggesting a higher flux of electrons through the respiratory chain at the Complex I
176 level.
177
178 Mitochondrial calcium loading capacity
179 To assess mitochondrial calcium handling, we measured the sensitivity of each mitochondrial preparation to
180 undergo the calcium-induced mPTP. Heart mitochondria from DOX-treated animals showed no alteration
181 neither in calcium retention time nor release rate regardless of the respiratory substrate used (Fig. 4a).
182 Similarly, no treatment-related effects on calcium flux were observed in kidney mitochondria (Fig. 4c).
183 However, liver mitochondria from DOX-treated animals showed an apparent decreased sensitivity to mPTP
184 opening (Fig. 4b). Hepatic mitochondrial preparations retained calcium for 43 ± 30% longer with Complex I-
185 linked respiration and 36 ± 19% for Complex II-linked respiration compared to control group although no
186 statistical significance was observed (p = 0.194 and 0.098, respectively). In addition, calcium release rates
187 were decreased by 49 ± 19% with Complex I-linked respiration and 18 ± 27% with Complex II-linked
188 respiration. Significance was not always achieved due to the high variability in response to the treatment (Fig.
189 4b). Confirming that all previous mentioned alterations were related to the mPTP opening is the fact that pre-
190 incubation with CsA, the classic mPTP desensitizer (Broekemeier *et al.*, 1989) prevented calcium release
191 (Table 1).
192 Additionally, the same mitochondrial preparations were assessed for calcium-induced mitochondrial swelling
193 in similar conditions to those aforementioned. Corroborating the above results, heart mitochondria swelling
194 amplitude and swelling rate were not altered after acute treatment with DOX, regardless of the respiratory
195 substrate used (Fig. 5a). Likewise, in kidney mitochondria, amplitude and swelling rate were not different

196 from control (Fig. 5c). However, liver mitochondria from DOX-treated animals appear to have slower
197 swelling rate (6 ± 12% and 21 ± 37% for glutamate/malate and succinate, respectively; Fig. 5b) despite no
198 apparent change in swelling amplitude (20 ± 30% and 11 ± 31% for glutamate/malate and succinate,
199 respectively). As in calcium-loading capacity experiments, a high variability in response to the treatment was
200 observed for liver mitochondria preventing any statistical differences. CsA under the experimental swelling
201 conditions abolished all the effects, confirming the opening of the mPTP (Table 2).
202 Two major regulators of the mPTP are: cyclophilin D (Cyp-D) in the matrix and ANT in the inner membrane
203 (Silva *et al.*, 2018). Cyp-D protein levels remained constant after the acute treatment regardless of the tissue
204 analyzed (Table 3). We next measured mRNA and protein content of two ANT isoforms (Table 4). The 40 ±
205 6% cardiac-specific decrease of *ANT1* mRNA was significantly stronger than the effects observed in liver and
206 kidney. Similarly, the 26 ±6% decrease of *ANT2* mRNA was significant when compared to kidney. Still, no
207 change in protein levels were observed after the 24 h treatment (Table 3). Moreover, no treatment- or tissue-
208 specific effects were detected regarding the protein and mRNA levels of VDAC, a porin of the outer
209 mitochondrial membrane which governs ion and metabolites flux into mitochondria (Table 4).
210 Overall, the sensitivity to mPTP opening remains constant in heart mitochondria after the acute treatment in
211 contrast with liver mitochondria which show strong resistance to mPTP opening. However, this mPTP
212 modulation cannot be attributed to changes in the protein levels of mPTP-related proteins. We suggest instead
213 that increased electron flux through the respiratory chain in liver mitochondria is modulating mPTP opening.
214

DISCUSSION

The mechanisms underlying DOX-selective cardiotoxicity remain undefined. Nevertheless, it is being more widely accepted that the antitumor activity is independent of cardiac toxicity, which may involve alterations of mitochondrial function (discussed in Pereira *et al.* (2011)). Acute DOX cardiac toxicity occurs during the early treatment of patients (high dose) and usually include symptoms which are therapeutically easy to manage and resolve once treatment is discontinued (Tokarska-Schlattner *et al.*, 2006). Alternatively, a small, but significant number of patients develop chronic cardiotoxicity that can manifest itself at the end of treatment or several years later (Steinherz, et al., 1991). However, unlike acute toxicity, the dose-dependence together with its difficult early detection, renders DOX chronic toxicity life-threatening and largely uncontrolled.

Regardless the mechanism(s) involved in DOX cardiotoxicity, the available data not only demonstrates mitochondrial involvement (Zhou, et al., 2001c), but also differences related to each treatment protocol (acute vs. sub-chronic in Pereira, et al. (2012)). Previously, by using Wistar rats treated with a single dose of DOX (20 mg/Kg), Ascensão et al. (2006; 2011; 2005) observed that heart mitochondria respiration and phosphorylation capacity were impaired after 24 h treatment. In contrast, we applied the same treatment protocol in younger rats of the same strain and observed no DOX effects on cardiac mitochondrial respiration, although minor, but statistical significant alterations were measured in ADP-stimulated respiration in liver (increase) and kidney (decreased) mitochondria (Pereira, et al., 2012), suggesting a differential response to DOX determined by age at time of treatment. Considering that a very large proportion of children with cancer are treated with DOX (van Dalen *et al.*, 2009) despite its potential cardiotoxicity, it is relevant to identify early alterations of mitochondrial parameters/markers, which can be considered as early cardiac-specific stress responses to drug treatment.

It has been demonstrated in different rat models that DOX sub-chronic treatment causes inhibition of mitochondrial respiration; oxidation of proteins, lipids, and nuclei acids; loss of cardiolipin and, alterations in the antioxidant enzymatic network (Oliveira *et al.*, 2004; Oliveira *et al.*, 2006; Pereira, et al., 2016; Wallace, 1986; Zhou, et al., 2001b). Alterations of mitochondrial activity were also reported in different cardiac-like cell models, associated to increased cell death (Asensio-Lopez *et al.*, 2016; Cunha-Oliveira *et al.*, 2018; Sardao *et al.*, 2009). Taking these sub-chronic markers of DOX toxicity into account we selected and

243 measured relevant mitochondrial mRNA and protein content, respiratory chain-derived H_2O_2, and calcium-
244 loading capacity in16-weeks old Wistar rats, suspecting that they would be reliable markers of DOX acute
245 toxicity.
246 Our data on calcium-loading capacity suggests that liver mitochondria are resistant to mPTP opening after
247 DOX treatment in agreement with the increased mitochondrial bioenergetics fitness previously described by
248 our lab (Ascensao, et al., 2011; Pereira, et al., 2012). Similarly, liver mitochondria displayed increased H_2O_2
249 production when mitochondria were stressed by using OXPHOS inhibitors. Together with the improved
250 mitochondrial fitness previously described, it suggests an increased electron flow through the respiratory
251 chain. Electron flow has also been reported to modulate mPTP sensitivity (Fontaine *et al.*, 1998),
252 corroborating our data from calcium-loading capacity experiments. However, because a single timepoint was
253 evaluated in our experimental setup (24 h), it was not possible to determine if DOX effect in liver
254 mitochondria is slow to develop or long-lasting.
255 Considering that increased mitochondrial oxidative stress and loss of calcium-loading capacity are
256 regarded as hallmarks of chronic DOX-induced cardiac mitochondrionopathy (Pereira, et al., 2011; Zhou, et
257 al., 2001a; Zhou, et al., 2001b; Zhou, et al., 2001c), our negative results in respect to cardiac tissue suggest
258 that H_2O_2 generation and early loss of calcium-loading capacity following an acute DOX treatment are not
259 reliable markers for early DOX cardiotoxicity. Therefore, it is relevant to identify alternative mitochondrial
260 markers in order to recognize early functional or molecular signs of DOX-related cardiovascular toxicity.
261 To this end, we also performed mRNA and protein analysis for components relevant for the maintenance of
262 mitochondrial integrity and for OXPHOS. In general, mitochondrial-encoded transcripts showed minimal and
263 heterogeneous increase in their levels compared to nuclear-encoded transcripts, demonstrating a preferential
264 initial targeting of nuclear DNA. This is reminiscent of our previous data showing that DOX accumulates
265 rapidly in the nucleus (Sardao, et al., 2009). Although the number of commercially available antibodies which
266 worked in our setup was much lower than the total number of transcripts, we performed a similar analysis at
267 the protein level, with at least one protein from each complex, semi-quantified by Western Blotting. No
268 protein differences were found between saline and DOX-treated groups regardless of the analyzed tissue. This
269 could be due to higher turnover rates for mitochondrial proteins in rodents (Brunner *et al.*, 1968; Miwa *et al.*,

2008). Therefore, neither a direct correlation can be performed, nor treatment-related differences can be properly attributed through this analytic methodology.

We complemented the study with an alternative strategy to analyze mRNA and protein data. From the PCA analysis, we obtained a consistent separation between treatment groups in the heart for all four respiratory complexes, suggesting that the effect of the DOX administration is clearly detected in this tissue. The boundary is particularly well defined when analyzing Complex I which was previously indicated as being inhibited in DOX-induced cardiotoxicity (Santos, et al., 2002). As for the other tissues, clear separations occur just in specific complexes: in liver there is a clear separation in Complex II, whereas in kidney clear boundaries are visible in Complexes II and III. This differential response of DOX suggests that the impact of treatment can be easily distinguished between the cardiac and other tissues such as the liver or kidney. Contrary to the absence or minimal changes in cardiac mitochondrial function (mPTP sensitivity, H_2O_2 production and, respiration and oxidative stress markers (Pereira, et al., 2012)), the trends detected in the PCA study confirmed Complex I as the most promising target to detect acute mitochondrial changes resulting from DOX-treatment in the heart. Heart accumulates DOX slowly but to a higher extent than liver (Peters *et al.*, 1981) which could explain why DOX inhibitory effect on transcription was more easily detected in the heart, suggesting a tissue-specific concentration-dependent effect. Alternatively, these findings could be explained on the basis of tissue-specific stability of nuclear and mitochondrial-encoded mRNAs (Connor *et al.*, 1996), being cardiac mRNAs less stable compared to the other tissues. Nonetheless, our data suggests that the observed mitochondrial molecular alterations precede changes in mitochondrial function.

FCA allowed the identification of promising features that can be used for the detection of an acute toxicity. UQCRFS1 transcript and protein levels were involved in higher correlation changes in both kidney and heart. Complex III UQCRFS1subunit has been shown to be decreased in Barth syndrome animal models (Huang *et al.*, 2015), a pathology which is associated to the development of cardiomyopathy (Dudek *et al.*, 2017). In addition to *NDUFB8*, *NDUFS4* mRNA levels were also identified as features with high correlation changes in heart. Recently, Piekutowska-Abramczuk *et al.* (2018) reported *NDUFB8* as the underlying gene in childhood-onset of Leigh-like encephalomyopathy, observing decreased NDUFS4 protein levels and lower Complex I activity as well. Interestingly, NDUFS4 is an accessory subunit important in Complex I assembly while NDUFB8 is an integral structural component of Complex I essential for its function (Sanchez-Caballero

298 *et al.*, 2016). NDUFB8 is not involved in the catalytic activity of Complex I but is an essential component of
299 the membrane-anchor required for the full assembly of Complex I and contribute to the oligomerization of
300 Complex I with Complex III and IV (Wu *et al.*, 2016). Interestingly, we have previously suggested loss of
301 mitochondrial supercomplexes as a possible underlying event in DOX-chronic toxicity (Pereira, et al., 2016).
302 Our results indicate that an acute DOX treatment leads to alterations in proteins and transcripts related
303 with Complexes I, III and IV in the heart and kidney, with a special predominance for Complex I. The liver
304 tissue, on the other hand, showed minimal alterations in molecular features, while displaying positive
305 adjustments in terms of respiration and calcium loading capacity, two measures of functional changes.
306 By using sequential Principal Component Analysis and Feature Correlation Analysis, we demonstrated for
307 the first time alterations in sets of transcripts and proteins, but not in functional measurements, that might
308 serve as potential early acute markers of cardiac-specific mitochondrial toxicity, contributing to explain the
309 trajectory of DOX cardiac toxicity and to measure the efficacy of novel interventions aimed at minimizing
310 DOX cardiac liabilities in anti-cancer treatments (Pereira, et al., 2012; Pereira, et al., 2016). Nonetheless,
311 longer resting periods after DOX-acute treatment should be studied to determine when mitochondrial
312 functional impairments begin to be apparent in the different organs studied. Similarly, it remains to be
313 elucidated whether these molecular markers are detectable in the circulation of DOX-treated animals or
314 patients. Although mRNA has become a signature-based biomarker in cancer management, their use in
315 cardiovascular medicine is still in its earlier days; however, it would prove instrumental in the early detection
316 of DOX-induced cardiotoxicity in the clinic and could replace myocardial biopsies, an invasive procedure to
317 detect heart diseases.
318

ACKNOWLEDGMENTS

This work was supported by FEDER funds through the Operational Programme Competitiveness Factors - COMPETE and national funds by FCT - Foundation for Science and Technology under the projects PTDC/DTP-FTO/1180/2012, POCI-01-0145-FEDER-007440, PTDC/DTP-FTO/2433/2014, POCI-01-0145-FEDER-016659, and POCI-01-0145-FEDER-029297. The FCT also supported doctoral fellowships for GP (SFRH/BD/36938/2007) and the pos-doctoral fellowship for S.P. (SFRH/BPD/116061/2016).

ETHICAL APPROVAL

All applicable international, national, and/or institutional guidelines for the care and use of animals were followed. All procedures performed in animal studies were in accordance with the ethical standards of the CNC – Center for Neuroscience and Cell Biology and Medical School of the University of Coimbra.

MATERIALS AND METHODS

Reagents

DOX hydrochloride, (7S,9S)-7-[(2R,4S,5S,6S)-4-amino-5-hydroxy-6-methyloxan-2-yl]oxy-6,9,11-trihydroxy-9-(2-hydroxyacetyl)-4-methoxy-8,10-dihydro-7H-tetracene-5,12-dione hydrochloride, chemical purity ≥ 98%, was obtained from Sigma-Aldrich (Barcelona, Spain) and prepared in a sterile saline solution, NaCl 0.9% (pH 3.0, HCl) and stored at 4ºC for no longer than five days upon re-hydration. All other chemicals were of the highest commercially available grade of purity. Aqueous solutions were prepared in ultrapure (type I) water (Milli-Q Biocel A10 with pre-treatment via Elix 5, Millipore, Billerica, MA, USA). For non-aqueous solutions, ethanol (99.5%) or dimetylsulfoxide (DMSO), both from Sigma-Aldrich, were used as solvent.

Animal care

Animal handling was performed in accordance with the European Convention for the Protection of Vertebrate Animals used for Experimental and Other Scientific Purposes (CETS no.123) and Portuguese rules (DL 129/92). The procedures were approved by the CNC Committee for Animal Welfare and Protection. Animal handlers and the authors GCP, SPP, JM, AA and PJO are credited by the European Federation for Laboratory Animal Research (FELASA) category C for animal experimentation (accreditation no. 020/08).

Male Wistar rats, Crl:WI(Han), were purchased from Charles River (France) with 14 weeks of age, acclimated for 10-14 days prior to the initiation of experiments and maintained in the local animal house facility (CNC – School of Medicine, University of Coimbra, Coimbra, Portugal). Animals were group-housed in type III-H cages (Tecniplast, Italy) with irradiated corn cob grit bedding (Scobis Due, Mucedola, Italy) and environmental enrichment and under controlled environmental requirements (22ºC, 45-65% humidity, 15-20 air changes/hour, 12 h artificial light/dark cycle, noise level < 55 dB) and free access to standard rodent food (4RF21 GLP certificate, Mucedola, Italy) and acidified water (at pH 2.6 with HCl) *ad libitum*.

The experimental model was performed as previously described (Pereira, et al., 2012). Briefly, male Wistar-Han rats (N = 34) were randomly divided into two groups (n = 17 each group) and received a single intraperitoneal injection (i.p.) of DOX (20 mg/Kg of body weight) or an equivalent volume of vehicle solution (NaCl 0.9% pH 7, controls), 24 h before sacrifice.

All animals were injected during the light phase of the cycle and weighed at the beginning and end of the experimental treatment period (data available in Pereira, et al. (2012)). Non-fasted animals were euthanized in pairs by cervical dislocation followed by decapitation, to confirm death and exsanguination. Organs were immediately extracted from the body and quickly washed in appropriate ice-cold buffer before being weighed (data available in Pereira, et al. (2012)). Tissues intended for mRNA and protein analyses were stored separately in RNAlater (Applied Biosystems/Ambion, Austin, TX) at –80°C, accordingly to manufacturer guidelines.

Isolation of mitochondrial fraction

Mitochondria were isolated by a standard procedure currently used in our laboratory (Pereira, et al., 2012). Briefly, organs were excised and finely minced in ice-cold isolation medium containing 250 mM sucrose, 10 mM HEPES, 1 mM EGTA and 0.1% defatted BSA (pH 7.4, KOH). After washing the blood, organs were homogenized with a motor-driven Teflon Potter homogenizer. For the isolation of cardiac mitochondrial fractions, isolation medium was supplemented with 0.5 μg/mL of protease (Subtilisin A, Type VIII from *Bacillus licheniformis*, Sigma-Aldrich, Madrid, Spain). Protease was removed from the cardiac homogenate by centrifugation at 14,400 g for 10 min at 4°C and the pellet, essentially devoid of protease, was gently homogenized and resuspended to its original volume with a loose-fitting homogenizer. Subsequently, all homogenates were centrifuged at 750 g for 10 min at 4°C and the resulting supernatants at 10,000 g for 10 min. Mitochondrial pellet was resuspended using a paintbrush and centrifuged twice at 10,000 g for 10 min before obtaining a pure mitochondrial suspension. EGTA and defatted BSA were omitted from the final washing medium (pH 7.2, KOH). Mitochondrial protein was quantified by the biuret method using bovine serum albumin (BSA) as standard. Mitochondrial preparations were kept on ice during experiments, which were carried out after 20 min recovery period and within 5 h. The respiratory control ratio (RCR) values of the mitochondrial preparations were within the standard range, demonstrating a good coupling between respiration and ATP phosphorylation (Heart saline glutamate plus malate 4.6 ± 0.4, succinate 2.7 ± 0.2; Liver saline glutamate plus malate 9.5 ± 1.0, succinate 8.2 ± 1.5; Kidney saline glutamate plus malate 4.1 ± 0.3, succinate 3.5 ± 0.2; there was no statistical difference between saline vs. DOX group), previously reported in Pereira, et al. (2012).

386

387 Measurement of hydrogen peroxide

388 H_2O_2 generation was measured fluorimetrically using a modified method previously described by Barja
389 (2002). Briefly, the method consists in the use of homovanillic acid which reacts with H_2O_2 in the presence of
390 horseradish peroxidase to form the fluorescent dimer 2,2'-dihydroxy-3,3'-dimethoxydiphenyl-5,5'-diacetic
391 acid (λEx/λEm = 312/420 nm). Reactions (500 µL) were conducted in standard glass test tubes under constant
392 magnetic stirring and incubated in a water bath at 30°C. Small volumes of reactants were combined in the
393 following order to pre-added incubation medium (145 mM KCl, 30 mM Hepes [pH 7.4, KOH], 5 mM
394 KH_2PO_4, 3 mM $MgCl_2$, 100 µM EGTA, 0.1% fatty acid-free albumin) to reach the following concentrations:
395 0.125 µg mitochondrial protein, 6 U/mL horseradish peroxidase and 100 µM homovanillic acid. H_2O_2
396 production was determined in mitochondria energized with 5 mM glutamate/malate or 5 mM succinate. At
397 these concentrations, H_2O_2 production is not substrate-dependent. In some experiments, specific inhibitors for
398 Complex I (rotenone, 1 µM) or for Complex III (antimycin A, 0.5 µM) were used in combination with
399 respiratory substrates to block electron transport and maximize H_2O_2 production. Arbitrary fluorescence units
400 were converted to nmol H_2O_2 by extrapolation through a standard curve established by addition of known
401 amounts of H_2O_2 in the presence of horseradish peroxidase and homovanillic acid. Values were then
402 normalized to protein amount and expressed as nmol H_2O_2/15 min/mg protein.

403

404 Mitochondrial Calcium Accumulation

405 Extramitochondrial free Ca^{2+} was assayed by monitoring the variations in fluorescence of the hexapotassium
406 salt of the probe Calcium Green 5-N (Ca5GN; Invitrogen, Spain, C-3737), which increases its yield upon
407 binding to calcium, and as previously described (Rajdev *et al.*, 1993). Briefly, isolated mitochondrial fraction
408 (0.25 mg/mL cardiac, 0.75 mg/mL liver and kidney) were suspended in 2 mL of buffer containing 200 mM
409 sucrose, 10 mM Tris, 10 µM EGTA (to complex basal calcium), 5 mM KH_2PO_4 for cardiac mitochondria, or
410 1 mM KH_2PO_4 for liver and kidney mitochondria, combined with 812 nM of Ca5GN. After mitochondrial
411 energization with 2.5 mM glutamate plus malate (enabling mitochondrial energization through complex I) or
412 2.5 mM succinate in the presence of 1 µM rotenone (enabling mitochondrial energization through complex II)
413 a baseline of 60 seconds was obtained before the addition of a single pulse of calcium of 65-100 nmol, 50-100

nmol and 40-65 nmol for heart, liver and kidney mitochondria. Fluorescence was continuously recorded in a water-jacketed cuvette holder at 30°C using a PerkinElmer LS-55 fluorescence spectrometer (PerkinElmer Life and Analytical Sciences, Boston, MA) at λEx/λEm = 506/531 nm. Five nm slits were used for excitation and emission wavelengths. Adequate controls were performed to assess possible interferences in probe fluorescence, under either low or high calcium concentrations (no interferences were observed for the experimental conditions described). Possible interferences with DOX were discarded since its emission peaks at 550 nm, a higher wavelength than our emission filter; and, excitation peaks at 475 nm, meaning that only a small fraction of the drug could lower Ca5GN excitation at 506 nm. Cyclosporin A (CsA), a desensitizer of the mPTP (Broekemeier, et al., 1989), was used to confirm that the recorded event was related to the mPTP.

Calcium-induced mitochondrial swelling

Mitochondrial osmotic volume changes associated with the calcium-induced mPTP were assessed by turbidimetry (Halestrap *et al.*, 1990). The optical density was monitored at 540 nm with a Jasco V-560 spectrophotometer (Jasco Inc., Easton, MD, USA) equipped with a magnetic stirrer and a water-jacketed cuvette holder connected to a water bath set to 30°C. The assay was carried out in the same buffer as described above for calcium loading experiments, but at a protein concentration of 0.5 mg/mL (heart) or 1.0 mg/mL (liver and kidney) was used. After a 60 sec baseline, a single pulse of calcium of 20-50 nmol/mg protein or 10-50 nmol/mg protein was added to heart or liver and kidney mitochondria, respectively. Absorbance variations were recorded and analyzed with the manufacturer's software. The swelling amplitude presented in the graphs is defined as the difference in absorbance between the time-point that corresponds to half of the maximum swelling amplitude of the control record and the baseline before calcium addition (larger values mean greater sensitivity to mPTP). CsA was used to confirm that the recorded events were related to the mPTP.

Total RNA isolation

RNA was isolated using the RNeasy Mini Kit (Qiagen Inc., Valencia, CA). Briefly, 20 mg of each RNAlater-conserved frozen tissue was thawed and ground in a glass pestle homogenizer followed by further homogenization with a 27-gauge needle connected to a syringe. The purification was performed as described

in the manufacturer's RNA clean-up protocol, following its suggestions. RNA was quantified using a NanoDrop spectrophotometer (ThermoFisher Scientific Inc., Rockford, IL). RNA quality and purity were assessed by observing a spectral scan with a single prominent A260 peak and A260/A280 ratio greater than 2.

Protein extraction and Western blot

RNAlater-conserved frozen tissue (70-150 mg) was thawed and ground in a glass pestle homogenizer in a 10% (m/v) RIPA buffer (150 mM NaCl, 50 mMTris, pH 8.8, 0.5% sodium deoxycholate, 0.1% SDS, and 1% Igepal), supplemented with 5 µL/mg of tissue of protease inhibitors cocktail (P8340, Sigma-Aldrich Inc, St. Louis, MO, USA). The homogenate was then centrifuged at 14,000 g for 5 min to remove cellular debris. Protein concentration was determined by BCA Protein Assay Kit (Thermo Fisher Scientific Inc.) using BSA as standard. Extracted proteins were diluted in Laemmli buffer (BioRad Laboratories, Hercules, CA, USA) supplemented with 2% β-mercaptoethanol then boiled at 95ºC for 5 min. Equal amounts of protein (25 µg) were loaded into 12% polyacrylamide gels separated by SDS-PAGE. Then, proteins were transferred to PVDF membranes (Millipore, Billerica, Massachusetts, USA) at 100 V for 90 min, at 4ºC. Membranes were blocked with 0.25% of non-fat dry milk in Tris-buffered saline (154 mM NaCl, 50 mM Tris, pH 8.0) containing 0.1% Tween-20 (TBS-T) using the SNAP-id system (Millipore) with 10 min incubation. After washing twice with TBS-T in the same system, membranes were incubated with primary antibody directed against the respective protein (listed in Table S1) through traditional procedures, overnight at 4ºC. After washing twice in the SNAP-id system, membranes were incubated in this system with the respective alkaline phosphatase-linked secondary antibody (1:6000), prepared in TBS-T. The membranes were processed for protein detection using the Enhanced Chemi-Fluorescence system (ECF; GE Healthcare, Buckinghamshire, UK) and imaged with the Versa Doc imaging system (BioRad). The densities of each band were calculated with Quantity One Software (BioRad) and expressed as a percentage of control. The assay was standardized by re-probing the membranes for actin (#MAB1501, Milipore) immunoreactivity (1:10,000) to verify whether similar amounts of protein present in all lanes.

Real time qRT-PCR

cDNA was synthesized from extracted RNA (0.5–1.5 µg) using random primers along with the Omniscript Reverse Transcription Kit (Qiagen). All primers (Table S2) used for real time qRT-PCR were designed using

the web-based PrimerQuest software (Integrated DNA Technologies, Inc., Coralville, IA). Real time qRT-PCR was carried out using FastStart SYBR Green I Kit (Roche Diagnostics, Indianapolis, IN) with 10 µL reaction volume and performed in a LightCycler (Roche Diagnostics). Quantitation of gene expression was achieved by measuring target messenger RNA (mRNA) copy number against a 10-fold serial dilution of target-specific DNA standard ranging between 10^7 and 10^3 DNA copies. A target-specific DNA standard was prepared for each transcript by performing a 150 µl PCR reaction using HotstarTaq PCR Master Mix Kit (Qiagen) and cleaning the product using the Qiaquick PCR Purification Kit (Qiagen) The purified DNA standard was visualized by running a 100 ng aliquot on a 1.5% agarose gel and verifying that a single product of the proper size was present. The DNA standard was quantified spectrophotometrically using the NanoDrop ND1000 and diluted to a standard stock concentration of 5×10^9 DNA copies per microliter. 18S ribosomal RNA was used to normalize gene expression. Real-time qRT-PCR of control and treated samples for each gene was performed on the same run to minimize potential run to run variability.

Exploratory analysis and data statistical analysis

Results are shown as means ± SEM of the indicated number of experiments. Statistical significance between mean differences was determined using two-tailed Student's t test after normality and homogeneity of variances was access using a Shapiro-Wilk and Levene's test. Control group was matched against the treated group for each day to exclude the variability associated with mitochondrial isolation. In the specific case when seeking to ascertain whether changes between saline and DOX group in the heart are actually different from changes in other tissues, regardless of the inter-tissue baseline (i.e. for mRNA) data were analyzed by a two-way ANOVA with planned contrasts against the interaction between treatment and tissue so that significant relative changes (fold-change) are dependent on tissue. p-Values were thereafter adjusted for multiplicity using Šídák post-hoc test. Differences were considered significant if $p < 0.05$ and categorized accordingly to their interval of confidence. Statistical analyses were performed using Graph Pad Prism version 5.0 (GraphPad Software, Inc., San Diego, CA, USA), except of the two-way ANOVA, which was performed using JMP-SAS version 9.03 (SAS Campus Drive, Cary, NC, USA).

The exploratory analysis comprises the application of Feature Correlation Analysis (FCA) and Principal Component Analysis (PCA) methods. For both studies, samples with missing values were discarded. Standardization was applied to all the remaining features and the corresponding standard scores were used. FCA was performed using the Pearson correlation coefficients, whose values belong to the interval [-1, +1]: +1 signals a total positive linear correlation, 0 identifies no linear correlation and -1 refers to a total negative linear correlation. To simplify the analysis of the results, we consider just the absolute magnitude of change and created several graphical displays of the correlation matrices.

PCA was applied to find the two principal components that collectively explain most of the variability of the original set. The obtained eigenvectors were used to project the original samples in a set of 2D plots. Both FCA and PCA studies were performed using Python2, version 7. We relied on the Pandas package to load, store and transform the data (McKinney, 2010). The statistical analysis was performed using SciPy (Jones, 2001) and scikit-learn (Fabian Pedregosa, 2011). FCA correlation plots were created using Matplotlib and Biokit modules (Hunter, 2007). PCA scatter plots and density region charts were obtained with Orange Biolab (Demsar J, 2013).

REFERENCES

Ascensao, A., Ferreira, R., Oliveira, P. J., and Magalhaes, J. (2006). Effects of endurance training and acute Doxorubicin treatment on rat heart mitochondrial alterations induced by in vitro anoxia-reoxygenation. *Cardiovasc Toxicol* **6**(3-4), 159-72.

Ascensao, A., Lumini-Oliveira, J., Machado, N. G., Ferreira, R. M., Goncalves, I. O., Moreira, A. C., Marques, F., Sardao, V. A., Oliveira, P. J., and Magalhaes, J. (2011). Acute exercise protects against calcium-induced cardiac mitochondrial permeability transition pore opening in doxorubicin-treated rats. *Clin Sci (Lond)* **120**(1), 37-49.

Ascensao, A., Magalhaes, J., Soares, J. M., Ferreira, R., Neuparth, M. J., Marques, F., Oliveira, P. J., and Duarte, J. A. (2005). Moderate endurance training prevents doxorubicin-induced in vivo mitochondriopathy and reduces the development of cardiac apoptosis. *Am J Physiol Heart Circ Physiol* **289**(2), H722-31.

Ascensao, A., Oliveira, P. J., and Magalhaes, J. (2012). Exercise as a beneficial adjunct therapy during Doxorubicin treatment--role of mitochondria in cardioprotection. *Int J Cardiol* **156**(1), 4-10.

Asensio-Lopez, M. C., Soler, F., Sanchez-Mas, J., Pascual-Figal, D., Fernandez-Belda, F., and Lax, A. (2016). Early oxidative damage induced by doxorubicin: Source of production, protection by GKT137831 and effect on Ca(2+) transporters in HL-1 cardiomyocytes. *Arch Biochem Biophys* **594**, 26-36.

Barja, G. (2002). The quantitative measurement of H2O2 generation in isolated mitochondria. *J Bioenerg Biomembr* **34**(3), 227-33.

Broekemeier, K. M., Dempsey, M. E., and Pfeiffer, D. R. (1989). Cyclosporin A is a potent inhibitor of the inner membrane permeability transition in liver mitochondria. *J Biol Chem* **264**(14), 7826-30.

Brunner, G., and Neupert, W. (1968). Turnover of outer and inner membrane proteins of rat liver mitochondria. *FEBS Lett* **1**(3), 153-155.

Cappetta, D., De Angelis, A., Sapio, L., Prezioso, L., Illiano, M., Quaini, F., Rossi, F., Berrino, L., Naviglio, S., and Urbanek, K. (2017). Oxidative Stress and Cellular Response to Doxorubicin: A Common Factor in the Complex Milieu of Anthracycline Cardiotoxicity. *Oxid Med Cell Longev* **2017**, 1521020.

Chatterjee, K., Zhang, J., Honbo, N., and Karliner, J. S. (2010). Doxorubicin cardiomyopathy. *Cardiology* **115**(2), 155-62.

Childs, A. C., Phaneuf, S. L., Dirks, A. J., Phillips, T., and Leeuwenburgh, C. (2002). Doxorubicin treatment in vivo causes cytochrome C release and cardiomyocyte apoptosis, as well as increased mitochondrial efficiency, superoxide dismutase activity, and Bcl-2:Bax ratio. *Cancer Res* **62**(16), 4592-8.

Connor, M. K., Takahashi, M., and Hood, D. A. (1996). Tissue-specific stability of nuclear- and mitochondrially encoded mRNAs. *Arch Biochem Biophys* **333**(1), 103-8.

Cunha-Oliveira, T., Ferreira, L. L., Coelho, A. R., Deus, C. M., and Oliveira, P. J. (2018). Doxorubicin triggers bioenergetic failure and p53 activation in mouse stem cell-derived cardiomyocytes. *Toxicol Appl Pharmacol* **348**, 1-13.

Davies, K. J., and Doroshow, J. H. (1986). Redox cycling of anthracyclines by cardiac mitochondria. I. Anthracycline radical formation by NADH dehydrogenase. *J Biol Chem* **261**(7), 3060-7.

Demsar J, C. T., Erjavec A, Gorup C, Hocevar T, Milutinovic M, Mozina M, Polajnar M, Toplak M, Staric A, Stajdohar M, Umek L, Zagar L, Zbontar J, Zitnik M, Zupan B (2013). Orange: Data Mining Toolbox in Python. *Journal of Machine Learning Research* **14**(1), 2349-2353.

Dudek, J., and Maack, C. (2017). Barth syndrome cardiomyopathy. *Cardiovasc Res* doi: 10.1093/cvr/cvx014.

559 Fabian Pedregosa, G. V., Alexandre Gramfort, Vincent Michel, Bertrand Thirion, Olivier Grisel,
560 Mathieu Blondel, Peter Prettenhofer, Ron Weiss, Vincent Dubourg, Jake Vanderplas, Alexandre
561 Passos, David Cournapeau, Matthieu Brucher, Matthieu Perrot, Édouard Duchesnay (2011). Scikit-
562 learn: Machine Learning in Python. *Journal of Machine Learning Research* **12**, 2825-2830.
563 Fontaine, E., Eriksson, O., Ichas, F., and Bernardi, P. (1998). Regulation of the permeability
564 transition pore in skeletal muscle mitochondria. Modulation By electron flow through the
565 respiratory chain complex i. *J Biol Chem* **273**(20), 12662-8.
566 Halestrap, A. P., and Davidson, A. M. (1990). Inhibition of Ca2(+)-induced large-amplitude swelling
567 of liver and heart mitochondria by cyclosporin is probably caused by the inhibitor binding to
568 mitochondrial-matrix peptidyl-prolyl cis-trans isomerase and preventing it interacting with the
569 adenine nucleotide translocase. *Biochem J* **268**(1), 153-60.
570 Hayward, R., and Hydock, D. S. (2007). Doxorubicin cardiotoxicity in the rat: an in vivo
571 characterization. *J Am Assoc Lab Anim Sci* **46**(4), 20-32.
572 Huang, Y., Powers, C., Madala, S. K., Greis, K. D., Haffey, W. D., Towbin, J. A., Purevjav, E., Javadov,
573 S., Strauss, A. W., and Khuchua, Z. (2015). Cardiac metabolic pathways affected in the mouse
574 model of barth syndrome. *PLoS One* **10**(6), e0128561.
575 Hunter, J. D. (2007). Matplotlib: A 2D graphics environment. *Computing in science & engineering*
576 **9**(3), 90-95.
577 Jones, E. a. O., Travis and Peterson, Pearu (2001). SciPy: Open Source Scientific Tools for Python.
578 McKinney, W. Data Structures for Statistical Computing in Python2010, Vol. 445, pp. 51 - 56.
579 Miwa, S., Lawless, C., and von Zglinicki, T. (2008). Mitochondrial turnover in liver is fast in vivo and
580 is accelerated by dietary restriction: application of a simple dynamic model. *Aging Cell* **7**(6), 920-3.
581 Nair, A. B., and Jacob, S. (2016). A simple practice guide for dose conversion between animals and
582 human. *J Basic Clin Pharm* **7**(2), 27-31.
583 Oliveira, P. J., Bjork, J. A., Santos, M. S., Leino, R. L., Froberg, M. K., Moreno, A. J., and Wallace, K.
584 B. (2004). Carvedilol-mediated antioxidant protection against doxorubicin-induced cardiac
585 mitochondrial toxicity. *Toxicol Appl Pharmacol* **200**(2), 159-68.
586 Oliveira, P. J., Santos, M. S., and Wallace, K. B. (2006). Doxorubicin-induced thiol-dependent
587 alteration of cardiac mitochondrial permeability transition and respiration. *Biochemistry (Mosc)*
588 **71**(2), 194-9.
589 Pereira, G. C., Pereira, S. P., Pereira, C. V., Lumini, J. A., Magalhaes, J., Ascensao, A., Santos, M. S.,
590 Moreno, A. J., and Oliveira, P. J. (2012). Mitochondrionopathy phenotype in doxorubicin-treated
591 Wistar rats depends on treatment protocol and is cardiac-specific. *PLoS One* **7**(6), e38867.
592 Pereira, G. C., Pereira, S. P., Tavares, L. C., Carvalho, F. S., Magalhaes-Novais, S., Barbosa, I. A.,
593 Santos, M. S., Bjork, J., Moreno, A. J., Wallace, K. B*., et al.* (2016). Cardiac cytochrome c and
594 cardiolipin depletion during anthracycline-induced chronic depression of mitochondrial function.
595 *Mitochondrion* **30**, 95-104.
596 Pereira, G. C., Silva, A. M., Diogo, C. V., Carvalho, F. S., Monteiro, P., and Oliveira, P. J. (2011). Drug-
597 induced cardiac mitochondrial toxicity and protection: from doxorubicin to carvedilol. *Curr Pharm*
598 *Des* **17**(20), 2113-29.
599 Peters, J. H., Gordon, G. R., Kashiwase, D., and Acton, E. M. (1981). Tissue distribution of
600 doxorubicin and doxorubicinol in rats receiving multiple doses of doxorubicin. *Cancer Chemother*
601 *Pharmacol* **7**(1), 65-9.
602 Piekutowska-Abramczuk, D., Assouline, Z., Matakovic, L., Feichtinger, R. G., Konarikova, E.,
603 Jurkiewicz, E., Stawinski, P., Gusic, M., Koller, A., Pollak, A*., et al.* (2018). NDUFB8 Mutations Cause
604 Mitochondrial Complex I Deficiency in Individuals with Leigh-like Encephalomyopathy. *Am J Hum*
605 *Genet* **102**(3), 460-467.

606 Rajdev, S., and Reynolds, I. J. (1993). Calcium green-5N, a novel fluorescent probe for monitoring
607 high intracellular free Ca2+ concentrations associated with glutamate excitotoxicity in cultured rat
608 brain neurons. *Neurosci Lett* **162**(1-2), 149-52.
609 Sanchez-Caballero, L., Guerrero-Castillo, S., and Nijtmans, L. (2016). Unraveling the complexity of
610 mitochondrial complex I assembly: A dynamic process. *Biochim Biophys Acta* **1857**(7), 980-90.
611 Santos, D. L., Moreno, A. J., Leino, R. L., Froberg, M. K., and Wallace, K. B. (2002). Carvedilol
612 protects against doxorubicin-induced mitochondrial cardiomyopathy. *Toxicol Appl Pharmacol*
613 **185**(3), 218-27.
614 Sardao, V. A., Oliveira, P. J., Holy, J., Oliveira, C. R., and Wallace, K. B. (2009). Doxorubicin-induced
615 mitochondrial dysfunction is secondary to nuclear p53 activation in H9c2 cardiomyoblasts. *Cancer*
616 *Chemother Pharmacol* **64**(4), 811-27.
617 Silva, F. S. G., and Costa, C. F., and Marques, R. J., and Oliveira, P. J., and and Pereira, G. C. (2018).
618 Pharmacological Targeting of the Mitochondrial Permeability Transition Pore for Cardioprotection.
619 In *Mitochondrial Biology and Experimental Therapeutics* (P. J. Oliveira, Ed.), pp. 423--490. Springer
620 International Publishing, Cham.
621 Simunek, T., Sterba, M., Popelova, O., Adamcova, M., Hrdina, R., and Gersl, V. (2009).
622 Anthracycline-induced cardiotoxicity: overview of studies examining the roles of oxidative stress
623 and free cellular iron. *Pharmacol Rep* **61**(1), 154-71.
624 Singal, P. K., and Iliskovic, N. (1998). Doxorubicin-induced cardiomyopathy. *N Engl J Med* **339**(13),
625 900-5.
626 Solem, L. E., Heller, L. J., and Wallace, K. B. (1996). Dose-dependent increase in sensitivity to
627 calcium-induced mitochondrial dysfunction and cardiomyocyte cell injury by doxorubicin. *J Mol*
628 *Cell Cardiol* **28**(5), 1023-32.
629 Steinherz, L. J., Steinherz, P. G., Tan, C. T., Heller, G., and Murphy, M. L. (1991). Cardiac toxicity 4 to
630 20 years after completing anthracycline therapy. *JAMA* **266**(12), 1672-7.
631 Sterba, M., Popelova, O., Vavrova, A., Jirkovsky, E., Kovarikova, P., Gersl, V., and Simunek, T.
632 (2013). Oxidative stress, redox signaling, and metal chelation in anthracycline cardiotoxicity and
633 pharmacological cardioprotection. *Antioxid Redox Signal* **18**(8), 899-929.
634 Tokarska-Schlattner, M., Zaugg, M., Zuppinger, C., Wallimann, T., and Schlattner, U. (2006). New
635 insights into doxorubicin-induced cardiotoxicity: the critical role of cellular energetics. *J Mol Cell*
636 *Cardiol* **41**(3), 389-405.
637 van Dalen, E. C., Raphael, M. F., Caron, H. N., and Kremer, L. C. (2009). Treatment including
638 anthracyclines versus treatment not including anthracyclines for childhood cancer. *Cochrane*
639 *Database Syst Rev* doi: 10.1002/14651858.CD006647.pub2(1), CD006647.
640 Wallace, K. B. (1986). Nonenzymatic oxygen activation and stimulation of lipid peroxidation by
641 doxorubicin-copper. *Toxicol Appl Pharmacol* **86**(1), 69-79.
642 Wallace, K. B. (2007). Adriamycin-induced interference with cardiac mitochondrial calcium
643 homeostasis. *Cardiovasc Toxicol* **7**(2), 101-7.
644 Wu, M., Gu, J., Guo, R., Huang, Y., and Yang, M. (2016). Structure of Mammalian Respiratory
645 Supercomplex I1III2IV1. *Cell* **167**(6), 1598-1609 e10.
646 Zhou, S., Heller, L. J., and Wallace, K. B. (2001a). Interference with calcium-dependent
647 mitochondrial bioenergetics in cardiac myocytes isolated from doxorubicin-treated rats. *Toxicol*
648 *Appl Pharmacol* **175**(1), 60-7.
649 Zhou, S., Palmeira, C. M., and Wallace, K. B. (2001b). Doxorubicin-induced persistent oxidative
650 stress to cardiac myocytes. *Toxicol Lett* **121**(3), 151-7.
651 Zhou, S., Starkov, A., Froberg, M. K., Leino, R. L., and Wallace, K. B. (2001c). Cumulative and
652 irreversible cardiac mitochondrial dysfunction induced by doxorubicin. *Cancer Res* **61**(2), 771-7.

653

654

TABLES

Table 1 - Effect of cyclosporin A (CsA) on calcium-induced mPTP evaluated with Ca5GN.

Substrate	Treat.	Heart		Liver		Kidney	
		Diff. Means	Pooled SE	Diff. Means	Pooled SE	Diff. Means	Pooled SE
		% of inhibition					
		$n_{CsA} = 4$		$n_{CsA} = 6$		$n_{CsA} = 5$	
Glutamate/Malate	Saline	85.9**	25.0	107.0***	21.0	98.8***	17.0
	DOX	96.4**	24.6	101.0***	22.0	96.0**	24.4
Succinate	Saline	92.2*	37.2	72.6***	11.7	101.4**	23.7
	DOX	97.0*	39.6	100.0*	32.0	98.5**	21.9

Tabulated values represent the difference between means of groups in the absence of CsA and groups with CsA, e.g. saline-glutamate/malate vs. saline-glutamate/malate + CsA, and are expressed as relative percentage to the group without CsA. *, $p \leq 0.05$; **, $p \leq 0.01$ and ***, $p \leq 0.001$ vs. group with CsA, as evaluated by an unpaired Student's t test. Abbreviations: Exp. – experimental setup; Treat. - treatment; Diff. Means - difference between group means; Pooled SE - pooled standard error; nCsA - replicates number in CsA group.

Table 2 - Effect of CsA on calcium-induced mitochondrial swelling.

Substrate	Treat.	Heart		Liver		Kidney	
		Diff. Means	Pooled SE	Diff. Means	Pooled SE	Diff. Means	Pooled SE
		% of inhibition					
		$n_{CsA} = 4$		$n_{CsA} = 6$		$n_{CsA} = 5$	
Glutamate/Malate	Saline	80.6*	34.8	108.6***	24.8	87.0**	23.6
	DOX	76.6**	33.7	80.9**	22.2	90.7**	25.3
Succinate	Saline	91.6***	14.4	99.0***	38.3	88.0**	18.9
	DOX	93.8**	28.7	98.1*	29.3	87.3**	20.5

Tabulated values represent the difference between means of groups in the absence of CsA and groups with CsA, e.g. saline-glutamate/malate vs. saline-glutamate/malate + CsA, and are expressed as relative percentage to the group without CsA. *, $p \leq 0.05$; **, $p \leq 0.01$ and ***, $p \leq 0.001$ vs. group with CsA, as evaluated by an unpaired Student's t test. Abbreviations: Exp. – experimental setup; Treat. - treatment; Diff. Means - difference between group means; Pooled SE - pooled standard error; nCsA - replicates number in CsA group.

673 Table 3 - Effects of DOX treatment on protein content of mPTP-related proteins.

		ANT		VDAC		Cyp-D	
		Mean	SE	Mean	SE	Mean	SE
Heart	Saline	1.02	0.05	0.96	0.02	1.00	0.03
	DOX	0.97	0.08	1.04	0.05	1.01	0.02
Liver	Saline	0.97	0.08	1.00	0.10	1.00	0.07
	DOX	1.04	0.04	0.99	0.08	1.01	0.04
Kidney	Saline	1.02	0.05	0.95	0.11	1.06	0.04
	DOX	0.99	0.05	1.04	0.08	0.95	0.05

674

675 Protein levels data are presented as arbitrary units and represent densitometry analysis of western blot
676 membranes after image acquisition. Differences between treatment group means were evaluated by matched
677 pairs Student's t test. Abbreviations: A.U. - arbitrary units; SE - standard error.

678

679 Table 4 – Effects of DOX treatment on transcript level of mPTP-related proteins.

		ANT1		ANT2		VDAC1		VDAC2		VDAC3	
		Mean	SE	Mean	SE	Mean	SE	Mean	SE	Mean	SE
Heart	Saline	8.04×10^{-3}	5.35×10^{-4}	2.55×10^{-4}	1.51×10^{-5}	1.51×10^{-3}	2.33×10^{-4}	4.05×10^{-4}	3.14×10^{-5}	5.36×10^{-4}	3.72×10^{-5}
	DOX	$4.82\times10^{-3\,a}$	1.94×10^{-4}	$1.87\times10^{-4\,b}$	1.29×10^{-5}	9.85×10^{-4}	7.57×10^{-5}	2.96×10^{-4}	1.32×10^{-5}	4.57×10^{-4}	2.42×10^{-5}
Liver	Saline	1.96×10^{-4}	1.54×10^{-5}	1.08×10^{-3}	6.41×10^{-5}	2.33×10^{-3}	2.54×10^{-3}	3.05×10^{-4}	4.19×10^{-5}	8.57×10^{-4}	8.97×10^{-4}
	DOX	2.00×10^{-4}	1.03×10^{-5}	1.12×10^{-3}	8.38×10^{-5}	3.23×10^{-4}	2.32×10^{-4}	3.01×10^{-4}	2.10×10^{-5}	1.28×10^{-4}	5.98×10^{-5}
Kidney	Saline	2.36×10^{-3}	2.01×10^{-4}	5.18×10^{-3}	4.70×10^{-4}	5.77×10^{-4}	7.36×10^{-5}	1.32×10^{-4}	1.26×10^{-4}	1.85×10^{-4}	2.29×10^{-5}
	DOX	2.63×10^{-3}	2.45×10^{-4}	5.90×10^{-3}	4.53×10^{-4}	4.32×10^{-4}	8.80×10^{-5}	1.38×10^{-5}	1.12×10^{-5}	1.97×10^{-4}	2.25×10^{-5}

680

681 Total mRNA was extracted from each tissue and transcript levels were analyzed through RT-qPCR with the
682 transcript copy number being thereafter normalized to 18S copy number. Values are shown as transcript copy
683 number / 18S copy number. For statistical analysis, tabulated values were log transformed and differences in
684 fold-change of each tissue were detected by a two-way ANOVA with planned contrasts and adjusted for
685 multiple comparisons through the Sidak test. ***a*** , $p \leq 0.05$ Saline-DOX fold-change in heart vs liver and
686 Saline-DOX fold-change in heart vs. kidney; ***b*** , $p \leq 0.05$ Saline-DOX fold-change in heart vs. kidney. $n = 6$
687 for all tissues and both experimental setups. Abbreviations: SE - standard error.

688

689

690 **FIGURE SUBTITLES**

691 Fig. 1: PCA projection along the two principal components of the separation between DOX (red) and Saline
692 (blue) samples for Heart (a), Kidney (b) and Liver (c). The two class density colors identify the area of
693 influence of each group. The four panels in each figure display results obtained with each mitochondrial
694 respiratory complex. PCA was performed on transcripts (mRNA) of genes encoding proteins from
695 mitochondrial Complexes I-IV. The study was based on 12 samples (6 Saline and 6 DOX) and 13, 4, 6, and 7
696 transcripts for each one of the 4 respiratory complexes (I-IV), respectively. PCA was performed separately for
697 each combination of tissue and specific respiratory chain complex, to simplify the identification of situations
698 in which a clear boundary between the two treatment groups emerges.
699
700 Fig.2: Matrices with all correlation changes in the features that result from the administration of DOX: a -
701 Heart; b - Kidney; c - Liver. Blank cells indicate that there is no significant change in correlation levels
702 calculated before and after DOX treatment. Cells with circles identify sizable changes in the correlation value.
703 The area and shading of a circle are directly proportional to the absolute magnitude of change.
704
705 Fig. 3: Effects of DOX treatment on mitochondrial H_2O_2 production. After 15 min, end-point H_2O_2 levels
706 were measured fluorimetrically through reaction with homovalinic acid. a - heart; b - liver; c - kidney. Circles
707 represent means of treatment groups (saline in white circles; DOX in black circles) with SEM (error bars are
708 smaller than symbols when not visible). Differences between means of treatment were evaluated by matched
709 pairs Student's t test to exclude the variability related to mitochondrial. $*p \leq 0.05$ and $**p \leq 0.01$ vs saline
710 group of the same model. n = 8, 7 and 6 (heart, liver and kidney, respectively).
711
712 Fig. 4: Effects of DOX treatment on mitochondrial calcium-loading capacity. Ca^{2+} movements were evaluated
713 using the extramitochondrial fluorescent probe Ca5GN after addition of a single pulse of Ca^{2+}. The retention
714 time is defined by the time interval between the influx and efflux of Ca^{2+} whose fluorescence value equals the
715 peak half-height fluorescence upon addition of calcium (larger values mean less sensitivity to mPTP). a -
716 heart; b - liver; c - kidney. Bars represent means of treatment groups (saline in white bars; DOX in black bars)
717 with SEM. Differences between means of treatment groups were evaluated by matched pairs Student's t test

718 to exclude the variability related to mitochondrial isolation. $*p \leq 0.05$ and $**p \leq 0.01$ vs saline group. n = 10,
719 9 and 10 (heart, liver and kidney, respectively). GM, glutamate/malate; SUC, succinate.
720
721 Fig. 5: Effects of DOX treatment on calcium-induced mitochondrial swelling. Mitochondrial swelling was
722 evaluated by following the decrease in apparent absorbance of the mitochondrial suspension at 540 nm after
723 addition of a single pulse of Ca^{2+}. The swelling amplitude presented in the graphs is defined as the difference
724 in absorbance between the point which corresponds to half of the maximum swelling amplitude of the control
725 record and the maximum absorbance before calcium addition (larger values mean greater sensitivity to
726 mPTP). a - heart; b - liver; c - kidney. Bars represent means of treatment groups (saline in white bars; DOX in
727 black bars) with SEM. Differences between means of treatment groups were evaluated by matched pairs
728 Student's t test to exclude the variability related to mitochondrial isolation. $*p \leq 0.05$ vs saline group of the
729 same model. n = 10, 9 and 10 (heart, liver and kidney, respectively). GM, glutamate/malate; SUC, succinate.
730

731 Figure 1

732

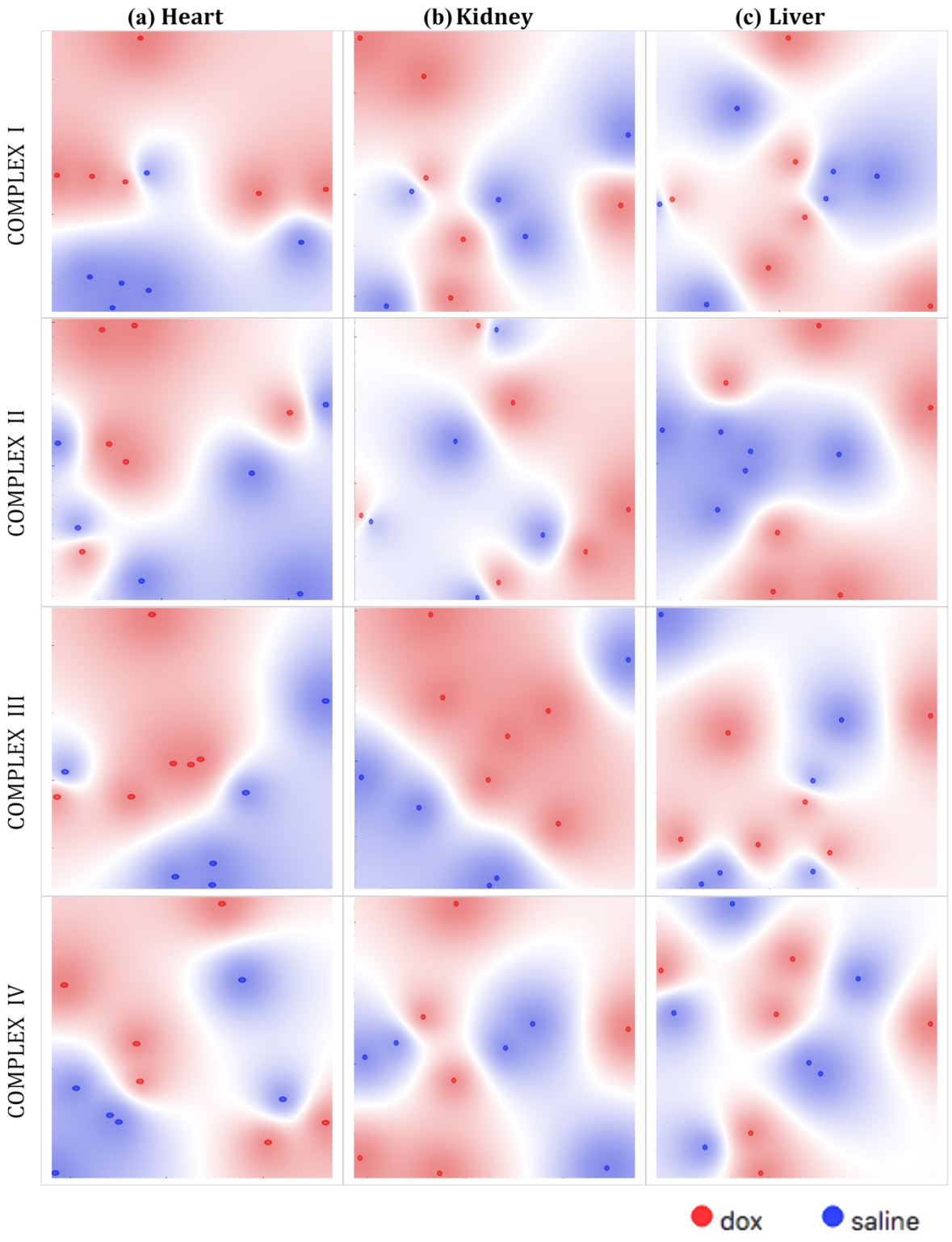

733

734 Figure 2A

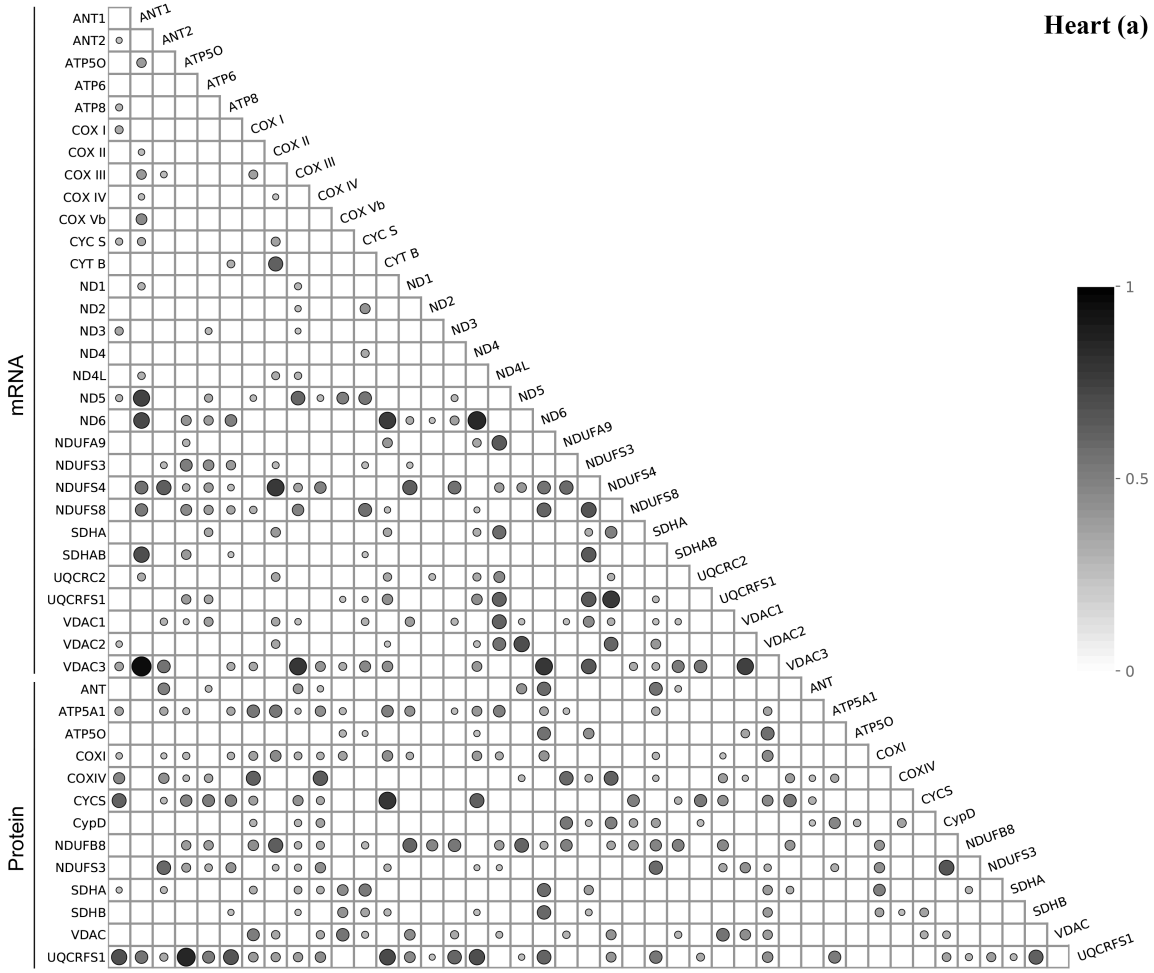

735

736

737 Figure 2B

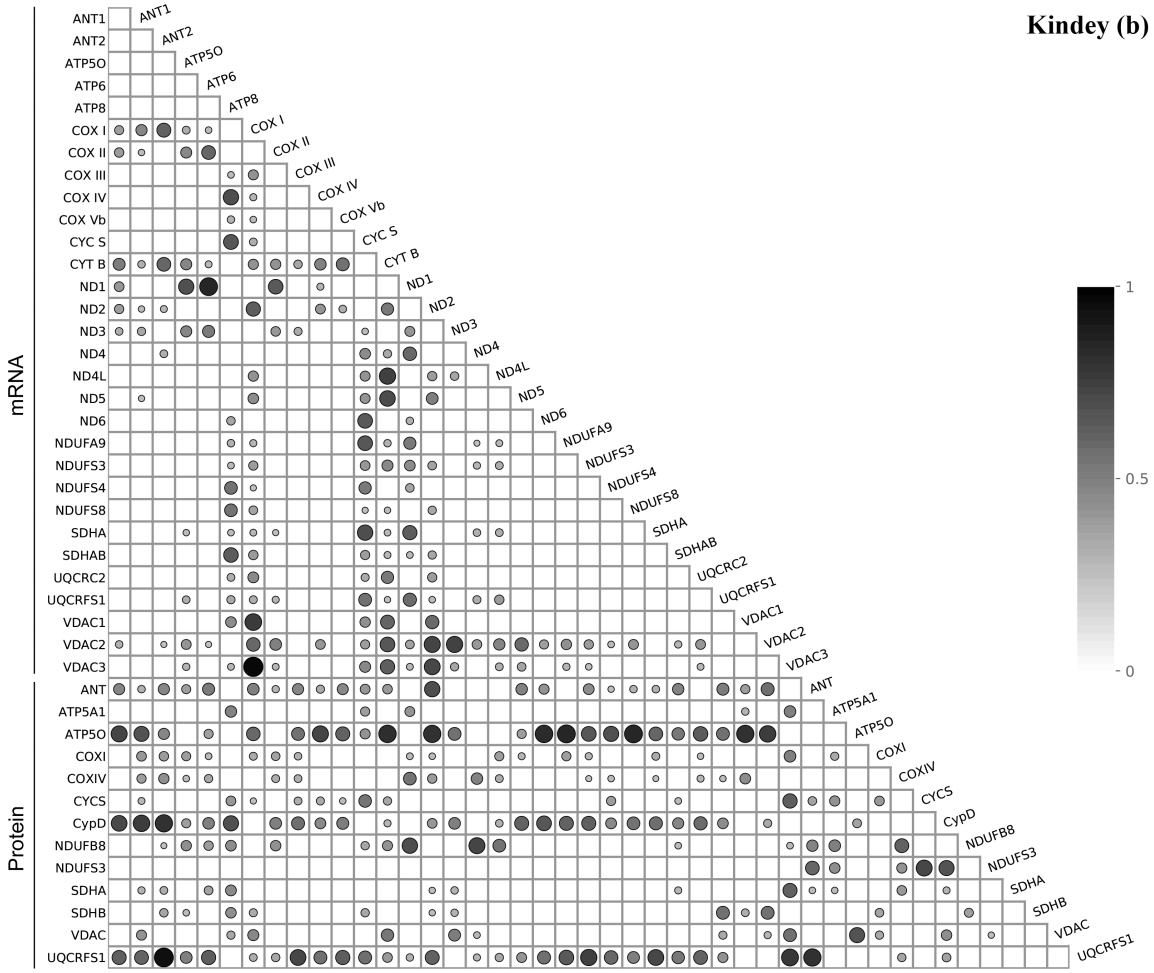

738

739

740 Figure 2C

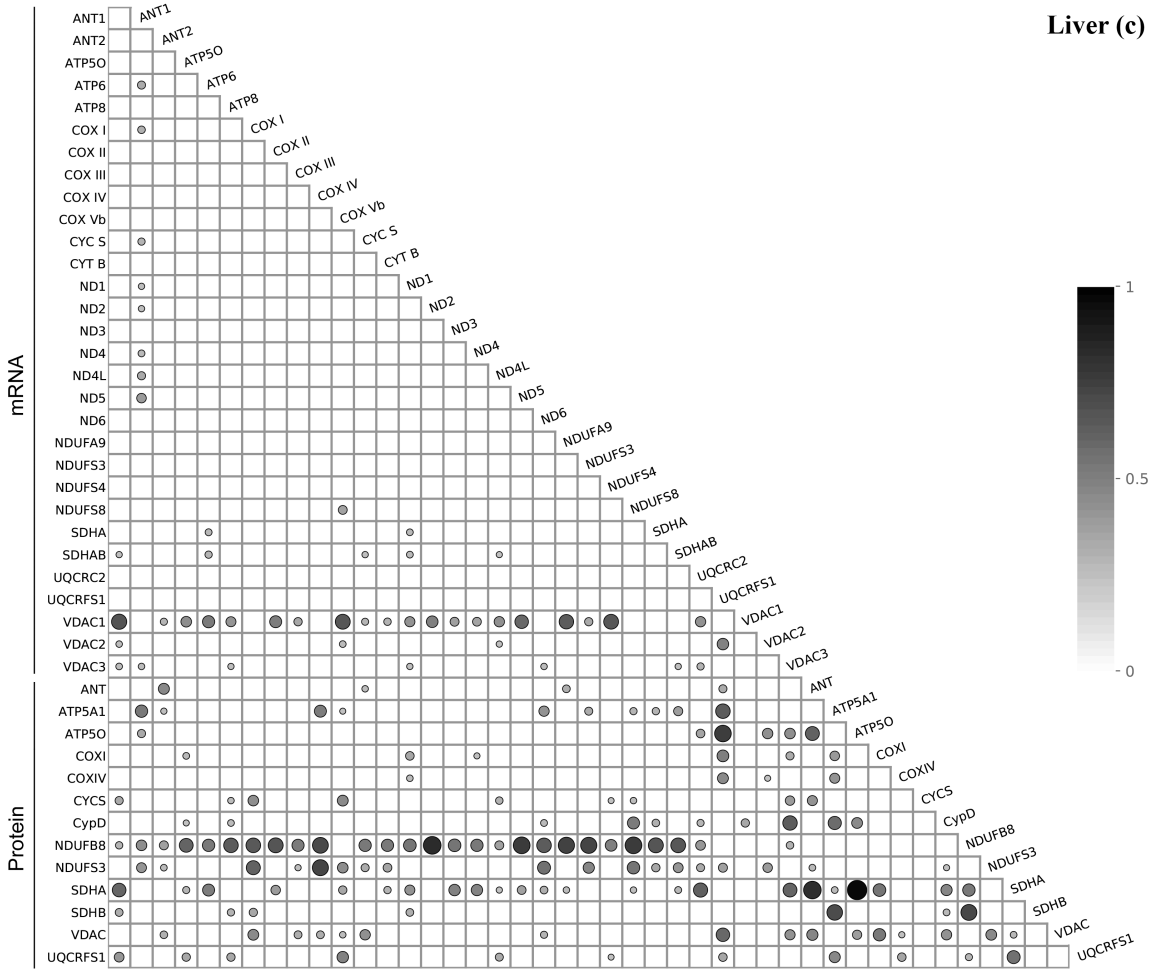

741

742

743 Figure 3

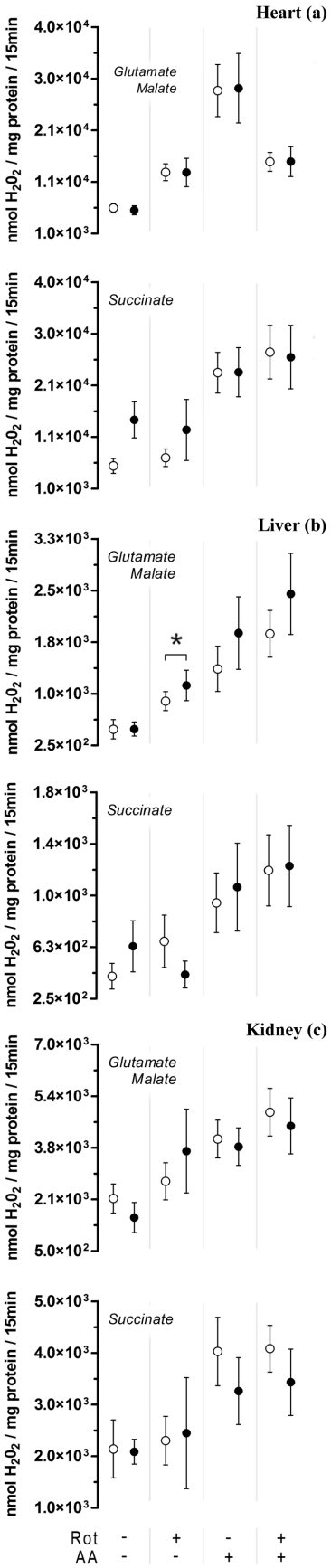
Heart (a)
Glutamate
Malate
Succinate
Liver (b)
Glutamate
Malate
Succinate
Kidney (c)
Glutamate
Malate
Succinate
nmol H_2O_2 / mg protein / 15min
4.0×10⁴
3.0×10⁴
2.1×10⁴
1.1×10⁴
1.0×10³
3.3×10³
2.5×10³
1.8×10³
1.0×10³
2.5×10²
1.8×10³
1.4×10³
1.0×10³
6.3×10²
2.5×10²
7.0×10³
5.4×10³
3.8×10³
2.1×10³
5.0×10²
5.0×10³
4.0×10³
3.0×10³
2.0×10³
1.0×10³
*
Rot - + - +
AA - - + +

745

746 Figure 4

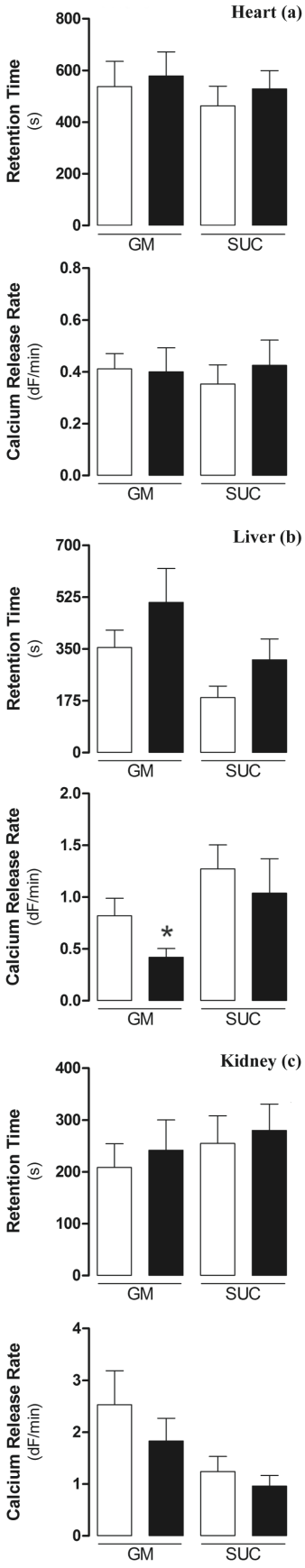
Heart (a)
Retention Time
(s)
800
600
400
200
0
GM
SUC
Calcium Release Rate
(dF/min)
0.8
0.6
0.4
0.2
0.0
GM
SUC
Liver (b)
Retention Time
(s)
700
525
350
175
0
GM
SUC
Calcium Release Rate
(dF/min)
2.0
1.5
1.0
0.5
0.0
*
GM
SUC
Kidney (c)
Retention Time
(s)
400
300
200
100
0
GM
SUC
Calcium Release Rate
(dF/min)
4
3
2
1
0
GM
SUC

748

749 Figure 5

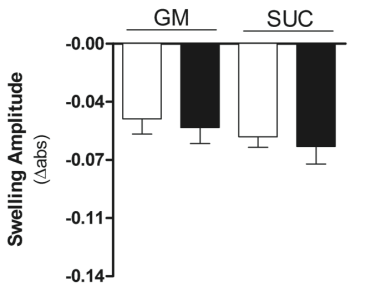

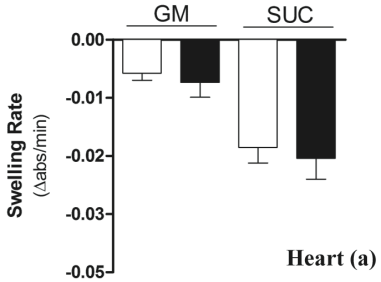

Heart (a)

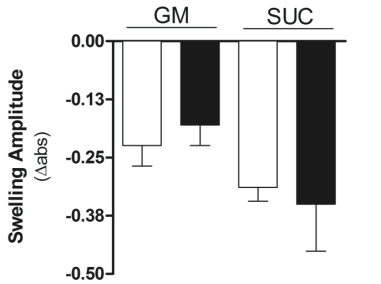

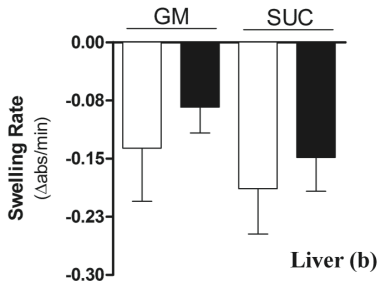

Liver (b)

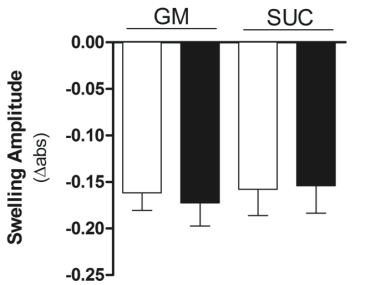

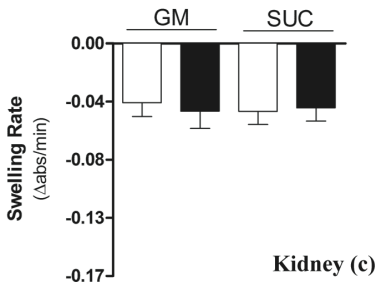

Kidney (c)

750